phys. stat. sol. (b) **222**, 219 (2000)

Subject classification: 61.72.Ji; S5.11

On the Properties of the Intrinsic Point Defects in Silicon: A Perspective from Crystal Growth and Wafer Processing

R. FALSTER[1]) (a), V. V. VORONKOV (b), and F. QUAST (c)

(a) MEMC Electronic Materials SpA, viale Gherzi 31, I-28100 Novara, Italy

(b) MEMC Electronic Materials SpA, via Nazionale 59, I-39012 Merano, Italy

(c) Fraunhofer-Institut für Integrierte Schaltungen, Bauelementetechnologie, Schottkystrasse 10, D-91058 Erlangen, Germany

(Received April 3, 2000)

Dedicated to Professor Dr. Wolfgang Schröter on the occasion of his 65th anniversary

Taking into account a wide variety of recent results from studies of silicon crystal growth and high temperature wafer heat treatments, a consistent picture of intrinsic point defect behavior is produced. The relevant point defect parameters: diffusivities, equilibrium concentrations and the details of the interaction of vacancies with oxygen are deduced. This set of parameters successfully explains a very wide array of experimental observations covering the temperature range 900–1410 °C. These experimental observations, which are reviewed here, include the properties of grown-in microdefects and vacancy-controlled oxygen precipitation effects in rapidly cooled wafers. The analysis of point defect behavior from observations of high temperature phenomena such as these has the great advantage of relative simplicity and transparency.

1. Introduction

Almost all defect phenomena and especially defect agglomeration in silicon have a component in which the intrinsic point defects play an important role. Several classes of agglomerated defect phenomena are particularly important to the performance of silicon in advanced Integrated Circuit (IC) applications. Examples are void formation during crystal growth and oxygen agglomeration both during crystal growth and in annealed wafers. Driven by the demand from the IC industry for higher performance, yet cost effective, silicon material to meet the requirements of the 1 Gbit era and beyond, significant progress has been made in the last few years. This progress has been both technological in the sense that new material/defect solutions have been found but also fundamental in the sense that consistent models for the various interconnected point defect reactions were developed. These reactions, in concert, produce a rich spectrum of defect phenomena in crystal growth and wafer processing. This paper sets out to describe in a general sense this interwoven tapestry of effects and the general building blocks of models which explain these effects in a detailed way. These models must consistently explain a wide variety of experimental observations from crystal growth and subsequent wafer processing. The variety of experimental evidence, covering a wide

[1]) Corresponding author; Tel.: +39 0321 334 394; Fax: +39 0321 691000;
e-mail: rfalster@memc.com

range of temperatures and combinations of effects, places a large number of constraints on any potential overall model for the important intrinsic point defect reactions, and on the values of the fundamental parameters of the intrinsic point defects used in these models. We begin with a review in general terms of the wide range of experimental observations and the outlines of the models that describe them. We then analyze this set of data and models together and discuss the self-consistent set of intrinsic point defect parameters which arises from the sum total of the constraints this places on them.

2. The Incorporation of Intrinsic Point Defects into a Growing Silicon Crystal

The most fundamental observation regarding intrinsic point defects and silicon crystal growth is that of a division of the growth of silicon crystals into two parts. These parts, those conditions under which a crystal is grown with either vacancies or silicon self-interstitials as the dominant native point defect, are determined by the value of the crystal growth parameter V/G, where V is the growth velocity and G is the temperature gradient near the melt–solid interface. At large values of V/G, the crystal is grown vacancy-type while at smaller values it is interstitial type. A critical value, denoted by ξ_{cr}, divides the two regimes. It is now generally accepted that a model developed by Voronkov in 1982 [1] correctly describes this effect. It is the problem of what is the survived – or incorporated – concentration of vacancies or self-interstitials in a growing crystal after it has been cooled from the melting point by some 100 K or so.

The positions of the contours of V/G in a growing crystal – and through them contours of incorporated vacancy and self-interstitial concentration – largely follow the contours of rich patterns of defect phenomena in silicon crystal. Banding of agglomerated defect types and densities and the oxygen precipitation behavior which is coupled to it are examples. Such patterns of defect behavior in silicon crystals can be made visible by a number of experimental techniques. Figure 1 illustrates one example (based

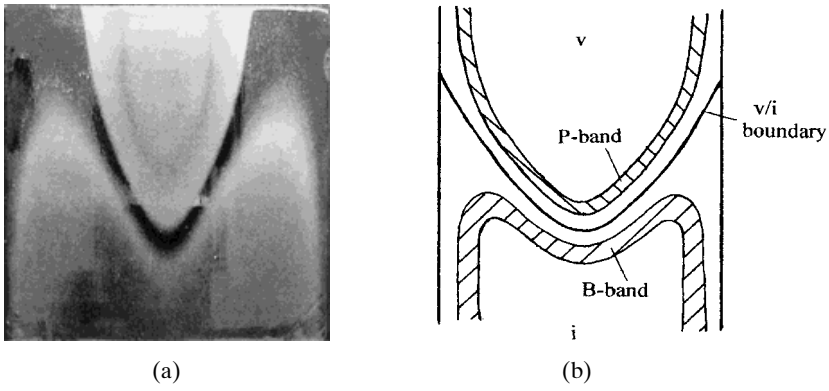

Fig. 1. Transition from vacancy to interstitial type material is achieved by reducing the crystal growth rate at constant $G(r)$. This is illustrated in a) an axial cross section of an etched Cu-decorated CZ crystal section at the transition from vacancy-type defect growth conditions (the upper "U-shaped" section) and interstitial-type defect conditions (the lower "M-shaped" structure). b) Schematic diagram of the structure of the transition near the critical V/G contours

on subsequent copper decoration) of the rich structure of intrinsic point defect patterns in silicon crystals. The nature of the defect bands will be briefly discussed below. The major division in the crystal is the division into vacancy and interstitial type, but there is considerable fine structure as well. In most cases, this is well described by a one-dimensional model which describes the competition between vacancies and self-interstitials. Only in some cases, especially near the crystal surface, two-dimensional models taking radial diffusion into account need to be applied to get satisfactory results.

Both vacancies and self-interstitials are present in comparable concentrations at the silicon melting point, T_m. On lowering T – that is, on moving away from the crystal/melt interface – the two defects recombine fast, thus creating strong concentration gradients, roughly proportional to the axial temperature gradient G in the near-interface region. Accordingly, there are appreciable diffusion fluxes of point defects directed from the interface into the crystal bulk which are proportional to G. They are added to the convection fluxes that correspond to defect transportation by a moving crystal. The convection flux is proportional to the growth rate V. At some distance from the interface only the defect with the larger flux survives to form a supersaturated solution and gives rise to microdefects on subsequent cooling. The concentration of the other defect decays rapidly. This defect solution is undersaturated.

If V/G is larger than ξ_{cr}, then the convection flux prevails over the diffusion flux, and the incorporated point defects are vacancies since they are of initially higher concentration. At T_m, the vacancy equilibrium concentration C_{Vm} is larger than that of interstitials, C_{Im}.

If V/G is less than ξ_{cr}, then the relative contribution of axial diffusion is increased, to make the in-flux of self-interstitials (the faster diffusers) prevailing. The incorporated point defects are then self-interstitials.

The critical ratio ξ_{cr} is a function of the point defect parameters at T_m [1, 2],

$$\xi_{cr} = (E/kT_m^2)\,(D_{Im}C_{Im} - D_{Vm}C_{Vm})/(C_{Vm} - C_{Im}), \tag{1}$$

where D_{Im} and D_{Vm} are the diffusivities at T_m and E is the average formation energy of the defects: $E = (E_I + E_V)/2$. Generally, the expression (1) includes also terms related to defect uphill drift (the drift rate is proportional to G), but these terms are not considered important [1, 2].

It is sometimes convenient to use the critical growth rate $V_{cr} = \xi_{cr}G$, to describe the change-over of the defect type – from self-interstitial at $V < V_{cr}$ to vacancy at $V > V_{cr}$. The incorporated concentration of vacancies, at $V > V_{cr}$, is defined by a simple general expression [2],

$$C_{Vs} = (C_{Vm} - C_{Im})\,(V - V_{cr})/(V + AV_{cr}), \tag{2}$$

where the coefficient A is close to 0.15. The expression (2) is applicable also for self-interstitials (at $V < V_{cr}$). It then defines the incorporated self-interstitial concentration C_{Is} with a minus sign.

The gradient G – and so the critical growth rate V_{cr} – is often of pronounced radial non-uniformity; it often increases strongly from the interface center to the periphery. This is, in essence, the origin of the radial non-uniformity of the crystal section shown in Fig. 1. At higher V the entire crystal cross-section becomes vacancy type, $V > V_{cr}$ everywhere. On the contrary, at lower V the entire crystal cross-section becomes interstitial type, $V < V_{cr}$ everywhere. At some intermediate range of V the inequality $V > V_{cr}$

is fulfilled only within a central part of the interface, while $V < V_{cr}$ at the periphery. Accordingly, the crystal is of a 'mixed type'. Under these conditions it contains a vacancy core surrounded by an interstitial peripheral region. It is this V/I boundary between the two regions that is responsible for the pronounced spatial distribution of microdefects in Fig. 1. Particularly, this boundary can be (approximately) traced by formation of a so-called P-band or OISF-ring (oxidation-induced narrow ring of stacking faults [3]) as discussed below.

3. Vacancy-Type Microdefects

In the vacancy growth mode, at $V > V_{cr}$, the vacancy solution becomes strongly supersaturated on lowering T, and vacancy agglomerates (microdefects) are produced at a progressively increasing rate. The nucleation rate increases so fast that appreciable nucleation occurs only within a rather narrow temperature range around some well defined 'nucleation temperatures' T_n [4]. At T larger than T_n the nucleation rate is still extremely low, while below T_n it decreases rapidly, due to vacancy loss to previously nucleated agglomerates. The nucleation temperature is typically around 1100 °C [5, 6] for the usual conditions under which CZ silicon crystals are grown.

3.1 Voids

It is now well established that the vacancy agglomerates formed in the standard mode are voids [7]. The void density N_v is typically about 2×10^6 cm^{-3} and the effective void radius R_v (that of a sphere of the same volume) is about 80 nm. Generally, the void density depends strongly on the cooling rate $q = -\mathrm{d}T/\mathrm{d}t$ through the narrow temperature interval of nucleation (at T_n). If the vacancy consumption by voids is limited by diffusion, the predicted dependence [4] of N_v on the cooling rate is $q^{1.5}$. This law well corresponds to the experimental $N_v(q)$ function measured in [6].

Voids are known to cause failure of gate oxides. They are also of increasing importance in device geometries on the order of the void size, isolation failures and other topological faults [8] – hence the technological interest. A huge effort has been expended in the silicon industry in recent years to develop crystal growth processes which deliver satisfactory distribution of voids in large crystal ingots. Voids can be detected by various experimental techniques. Depending on the particular experimental technique employed, voids are sometimes referred to as D-defects, COPs (crystal originated particles), Flow Pattern Defects, Light Scattering Tomography Defects and GOI (gate oxide integrity) defects.

3.2 P-bands

Vacancies can also form joint agglomerates with oxygen atoms – in other words, small oxide particles (in CZ, as opposed to FZ, crystals that is, where oxygen is present in appreciable amounts). In this reaction, vacancies and oxygen atoms act as the two chemical constituents of the produced microdefect (an oxide particle). At the same time, vacancies provide space for oxide particles, otherwise the strain energy would be prohibitively large for nucleation at these high temperatures. Since vacancies are not the only constituent of these particles, the particle nucleation is not as sensitive to the vacancy concentration C_V as that of voids. Accordingly, the ratio of the two nucleation rates, of particles to voids, increases very rapidly upon lowering C_V. At low incorporated vacancy

concentration (at V only slightly larger than V_{cr}) oxide particles are formed instead of voids [4]. This means that the vacancy region of a crystal is generally subdivided into a major inner portion (containing voids) and a narrow marginal band (where C_V is low) containing oxide particles. This 'P-band' gives rise to a well-known narrow ring of oxidation-induced stacking faults (OISF-ring) in oxidized wafers. Stacking faults are heterogeneously nucleated at these oxide particles [3]. The OISF-ring is therefore a good marker of the I/V boundary in mixed-type crystals; though it is located not precisely at the I/V boundary, but shifted somewhat towards the vacancy region.

3.3 L-bands and vacancy enhanced oxygen precipitation

At still lower vacancy concentration the particle nucleation is shifted to lower T, where oxygen diffusivity is reduced. Accordingly, particle growth becomes so slow that vacancy consumption is not significant. The P-band is therefore surrounded with another narrow band containing unconsumed vacancies. Here the vacancy concentration remains close to the originally incorporated value, C_{Vs}. This outer band of the vacancy region is called 'L-band' [9, 10]. Normally this band, outside the P-band, is narrow but well pronounced in oxygen precipitation maps. An example is shown in Fig. 2. The precipitation pattern (after a two-step anneal, 800 °C + 1000 °C) was revealed by life-

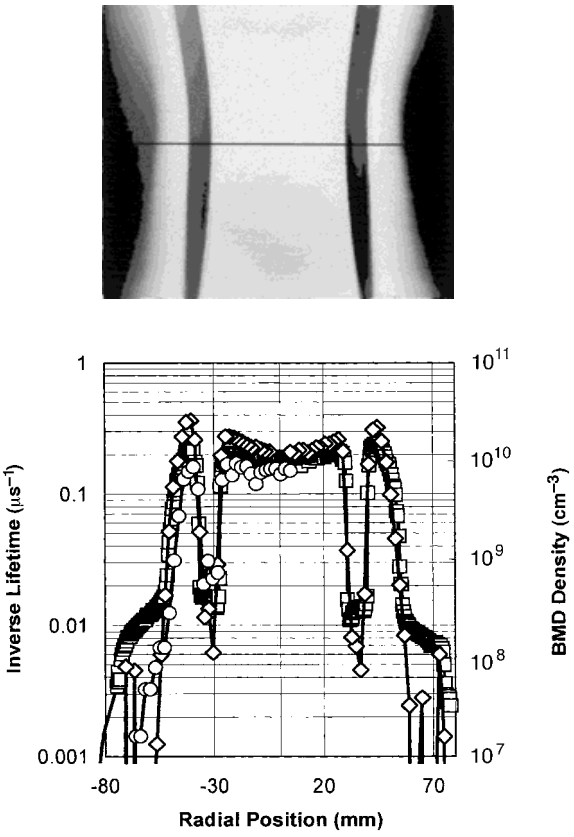

Fig. 2. Reactions which govern the subsequent nucleation of oxygen precipitates coupled to the reactions which produce intrinsic point defect agglomerates. This is illustrated by analysing the oxygen precipitation behaviour near a V/I transition. a) Minority carrier lifetime map of a longitudinal crystal section containing a V/I boundary after a two-step precipitation anneal (800 °C/4 h + 1000 °C/16 h). b) Radial variation of inverse lifetime and BMD density calculated from oxygen loss measurements (N:FTIR) and measured by infrared scattering microscopy (N:SIRM). The p-bands are located at about +/− 30 mm (□ $1/\tau$, ◇ N:FTIR, ○ N:SIRM)

time mapping and precipitate density determination. The precipitation nuclei (oxygen clusters) are formed in the middle-temperature range (around 650 °C) during subsequent crystal cooling. Oxide cluster formation is strongly enhanced by relatively large concentration of unconsumed vacancies in this band. The vacancy effect on oxygen precipitation will be discussed later in more detail.

Generally some small fraction of initially incorporated vacancies is left in the crystal, not only in the marginal L-band but also in the P-band and in the inner void region. The residual vacancy concentration in the P-band is very, very low, due to a high local density of vacancy consumers, the oxide particles. In the neighboring void region, the residual vacancy concentration is much larger, since the density of vacancy consumers, voids, is not as large. For this reason, the residual vacancy concentration C_{res} as a function of the initially incorporated concentration C_{Vs}, has a well-pronounced minimum corresponding to the P-band [9]. The lack of sufficiently large vacancy concentration in the P-band region results in the suppression of oxide cluster formation at lower temperatures. In the pattern of Fig. 2 the P-band is a black band of lower densities of precipitates. The density of oxide precipitates found in this region (following a precipitation anneal) is thus limited to the density of precipitates originally formed during the high temperature phase. In this example, the density of grown-in oxide particles is lower – as it almost always is in practical situations – than the density of the precipitate nuclei which then subsequently grow into particles upon further treatment in the other higher residual vacancy concentration regions. In self-interstitial dominant regions of silicon crystals, the lower temperature oxide clustering is completely suppressed. Oxygen precipitation maps are thus often very good general maps of residual vacancy concentration contours and V/I boundaries.

The concentration of residual vacancies necessary to produce the remarkably enhanced precipitation effect is thought to be about 10^{12} cm $^{-3}$ (see the discussion below). Such residual concentrations can be achieved, for example, by quenching a vacancy-type crystal through the conditions where normal void growth (and hence vacancy consumption) would occur. This often happens in the tail end of CZ crystals as a result of rapid extraction of the crystal following the completion of full diameter part of the crystal growth process.

3.4 Binding of vacancies by oxygen

It should be noted that survival of some vacancies – to facilitate oxygen clustering at 650 °C – is largely based on the reaction of vacancy binding to oxygen. The binding energy of an oxygen to a vacancy is high, since an oxygen atom moves from a double-bonded position between the two silicon neighbors to a similarly bonded state within a vacancy, and one silicon–silicon bond is restored in this reaction. Binding becomes significant below some binding temperature T_b (estimated to be about 1020 °C). The corresponding reduction in the effective vacancy mobility prevents some fraction of the vacancies from complete consumption by voids. Without binding, the vacancy consumption by voids would continue efficiently as the crystal cools, thus reducing their concentration to a negligibly small value, even in "quenched" crystals.

At temperatures larger than T_b, vacancy point defects are mostly monovacancies; the fraction of bound vacancies OV and O_2V is small. Void nucleation normally occurs at T_n, well above T_b, and so it is not much affected by the binding effect.

At T less than T_b, the vacancy point defects exist predominantly as vacancy–oxygen complexes, O_2V [9], since each of the pair of vacancy dangling bonds acquires an oxy-

gen atom. Therefore, in the effect of vacancy-enhanced precipitation around 650 °C, we actually deal with bound vacancies O_2V, vacancy–oxygen complexes. For the sake of brevity, we will refer to these species simply as vacancies, while bearing in mind that these are actually bound vacancies.

4. Interstitial-Type Microdefects

Historically, the agglomeration of self-interstitials was studied first [11], since dislocation-free silicon crystals were initially grown in the interstitial mode. There is a remarkable similarity in the formation of interstitial-type and vacancy-type microdefects.

At higher incorporated interstitial concentration C_{Is} (at V well below V_{cr}) interstitial-type dislocation loops are formed. They are also referred to as A-swirls or Large Etch Pit defects. Their density is considerably less than that of voids. This feature results mainly from a higher interstitial diffusivity. A smaller microdefect density is sufficient to efficiently consume self-interstitials and thus stop further nucleation. The loop size is, however, much larger than that of voids, both due to the lower microdefect density and to flat geometry. The larger size and nature of the defect type means that the A-defects may be even more harmful to devices than voids.

At lower C_{Is}, loops are replaced by smaller microdefects known as B-swirls. This is quite similar to replacement of voids with oxide particles at low C_{Vs}, and the reason is likely to be similar: a competition between two kinds of agglomerates. For instance, B-defects may be joint agglomerates of self-interstitials and carbon interstitials; the latter are produced by kick-out reaction from substitutional carbon. Neither the structure of B-swirls nor their impact on the devices is clear at present.

5. Vacancy Incorporation and Reaction in Crystal Growth: A Summary

The major components of the system which produces the vacancy reactions observed can be illustrated schematically. This is done in Fig. 3. It illustrates what might be called the basic vacancy *reaction template*. Here the various important zones of vacancy reac-

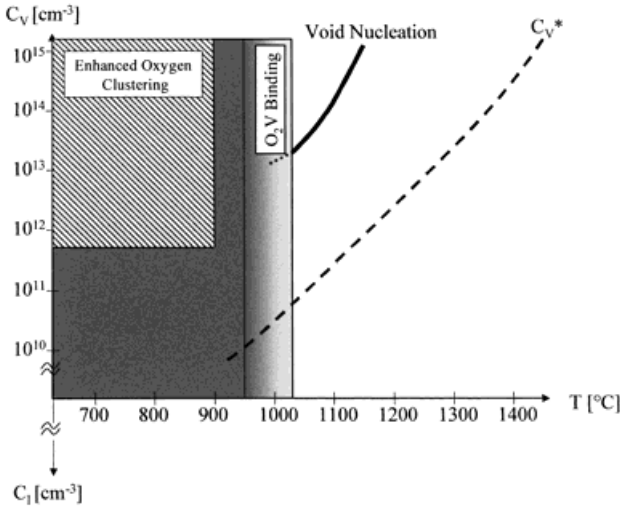

Fig. 3. Basic vacancy reaction "template". This diagram, which forms the basis of others which follow, illustrates those features important for the incorporation or reaction of vacancies in silicon at elevated temperatures. The line labeled C_V^* represents the equilibrium concentration of vacancies in silicon. The line labeled "void nucleation" represents the critical vacancy concentration contour for void nucleation

tion (void formation, O_2V binding and enhanced oxygen precipitation) are plotted in terms of temperature and vacancy concentration. As a main point of reference, the solubility of vacancies is also shown. Such a chart can be viewed as a kind of map through which the concentration of vacancies in a growing crystal or heat-treated wafer must be steered during the cooling of the crystal or wafer in order to achieve a desired result.

In this section little regard will be shown to the actual values of the intrinsic point defect parameters required to produce the effects shown schematically here. This problem will be considered in some detail in a later section.

Figure 4 uses this map to illustrate the first part of the crystal growth problem: that of the incorporation of vacancies into a growing crystal. Starting at the equilibrium concentration at the melt temperature, the vacancy concentration is reduced as the crystal cools through a transient phase in which vacancy and self-interstitial fluxes compete with each other via mutual annihilation. Eventually this stops when the concentration of one or the other point defect species becomes exhausted. At this point an essentially constant concentration of the surviving species is obtained. It is the incorporated vacancy (or self-interstitial) concentration, set at high temperature by the V/G rule, which is then launched into the possible reactions at lower temperatures. The reference value of the ratio of the actual to critical V/G value is given on the right-hand scale for several examples. The reference value corresponds to the vacancy concentration for each curve at the saturated or "incorporated" concentration. At the normalized V/V_{cr} value of 0.8 the illustrated incorporated vacancy concentration drops below the equilibrium concentration. The crystal is at this point "interstitial type".

Figure 5 illustrates the most usual case in commercial CZ crystal growth, that of void reaction. At a temperature of typically around 1100 °C the vacancies incorporated in the growing crystal become sufficiently supersaturated to drive the reaction. Very shortly after this starts, a sufficiently large number of vacancies are consumed by the voids, thus shutting off the nucleation reaction. The resulting density of voids produced in this interval depends on the concentration of vacancies entering the reaction barrier

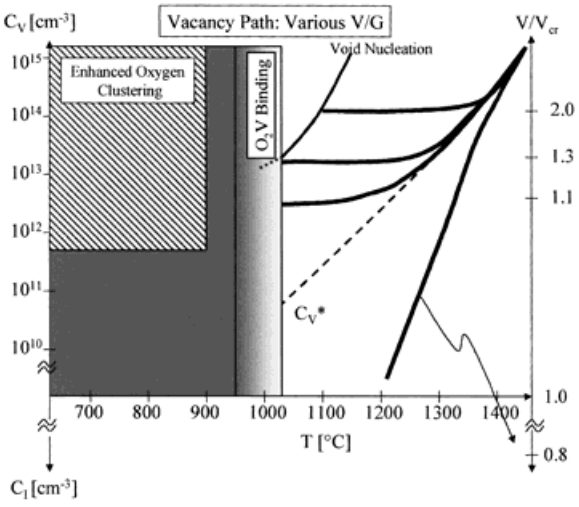

Fig. 4. Illustration of the incorporation of vacancies into a growing crystal. The reduction of vacancy concentration via recombination with self-interstitials during cooling from the melt temperature is illustrated for various values of V/G relative to the critical value. This ratio (given as V/V_{cr}) is shown on the right-hand scale. The specific value for each case corresponds to that at the saturated concentration level

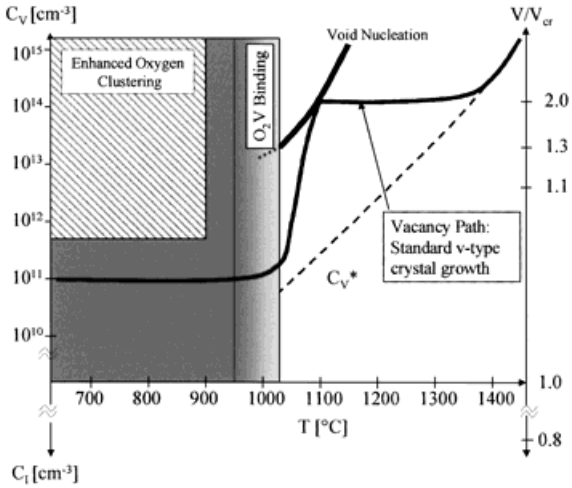

Fig. 5. Illustration of the production of voids in a growing crystal in the most usual case. In this case the cooling rate is sufficiently slow to allow for nucleated voids to consume vacancies to concentrations below that required for enhanced clustering prior to their "freezing" via O_2V complex formation

(proportional to $C_V^{-1/2}$ [4]) and the cooling rate while the reaction proceeds. Upon further lowering of the crystal temperature no more voids are produced but vacancies continue to be consumed by the existing voids until the remaining vacancies are fully bound in the relatively immobile O_2V complex. The residual concentration of vacancies (now in the form of O_2V complexes) is, however, usually below the critical concentration level for precipitation enhancement. In such cases of binding-limited void growth, the residual vacancy concentration becomes pinned at the vacancy equilibrium concentration near the binding temperature. Since this is the usual case, the residual vacancy concentration of most silicon crystals is thus roughly equal to this value. This is also true for the residual vacancy concentration in *wafers* following high temperature treatments and moderate cooling rates. Here the sinking sites are the wafer surfaces. The vacancy concentration in heat-treated wafers is discussed in some detail below. It is for this reason that measured oxygen precipitate nucleation rates in normal silicon wafers in properly controlled experiments are so reproducible. Fully satisfactory models (for the complete temperature and compositional dependence) of the nucleation of oxygen precipitates under these conditions remain illusive, however.

Returning to the problem of crystal growth: if, however, the crystal is cooled rapidly through the growth phase, such as can happen when fast pull rates are used to produce crystal end cones, the residual vacancy concentration can be larger than the transition level to enhanced oxygen precipitation. Regions of "anomalously" high levels of precipitation are observed under these conditions. Figure 6 illustrates this effect within the framework of the vacancy diagrams. Without the O_2V binding effect stopping the loss of vacancies to voids, under no circumstance could sufficiently high concentrations of residual vacancies be produced to enter into the precipitation enhancement regime during crystal growth.

At lower values of V/G, and in particular at values of V/G approaching the critical value, the concentration of incorporated vacancies is reduced. It is at these levels of vacancy concentration that strong defect banding effects are observed. Figure 7 illustrates the conditions for "P-band" or OISF-ring formation. The consumption rate of

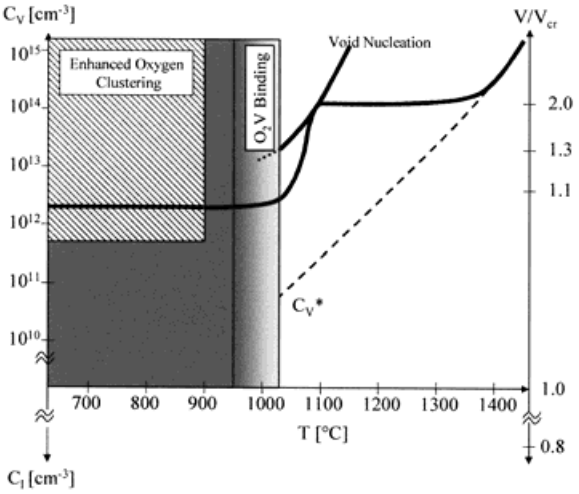

Fig. 6. Illustration of the effect of more rapid cooling through the void growth regime resulting in "anomalously" high values of oxygen precipitation. Here the cooling rate is sufficiently fast such that vacancy consumption by voids is insufficiently fast to suppress the concentration below the critical value for "enhanced clustering"

vacancies is larger than the void case due to the typically two orders of magnitude higher density of the P-band particles (the vacancy "sinks") than voids.

Figure 8 shows the case for "L-band" formation. In this case the vacancy concentration goes underneath the void or oxide particle reaction and enters directly into the O_2V binding as illustrated in Fig. 8. The usual case is for the vacancies to enter the "enhanced precipitation" condition at lower temperature giving rise to the precipitation peaks observed in the L-band region. Material grown under these conditions where vacancy reaction is stopped due to binding by oxygen contains no voids at all. Such material can be called "vacancy perfect" silicon – "perfect" in the sense that it is microdefect free. Another type of microdefect-free or "perfect" silicon can be produced on the interstitial side. The development of processes which steer the growth of large crystals through one or both of these two regimes represents an important advance in silicon crystal growth technology [12].

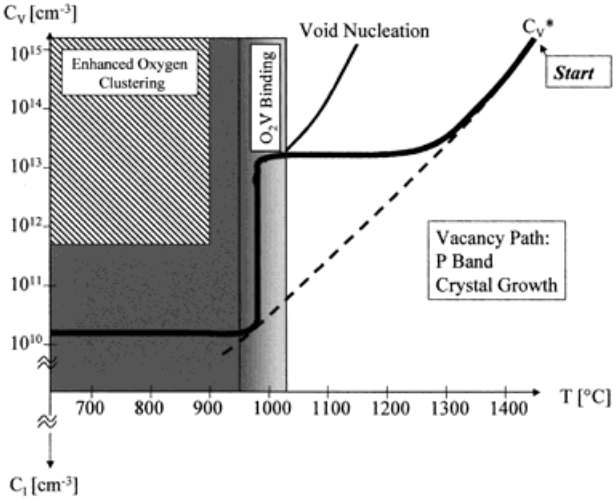

Fig. 7. Illustration of the conditions under which the "P-band" or OISF-ring is formed during crystal growth. Here the particle production path dominates over void production. Subsequent vacancy is very strong due to the higher densities of particles with respect to voids

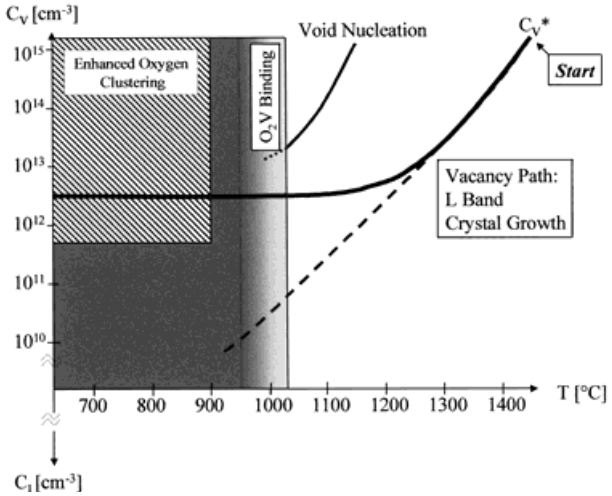

Fig. 8. Illustration of the conditions under which the "L-band" or "vacancy-perfect" type material is formed during crystal growth. Here the vacancy concentration set by the local *V*/*G* condition at the melt temperature is such they enter the binding regime before reacting to form voids

6. Intrinsic Point Defects and Reactions in Wafer Processing

6.1 The problem of oxygen precipitation in silicon wafers

The control of the behavior of oxygen in silicon *wafers* is one of the most important challenges in semiconductor materials engineering. Since the discovery of the internal gettering effect in silicon wafers, many scientists and engineers have struggled with the problem of precisely and reliably controlling the precipitation of oxygen during the processing of wafers into integrated circuits (ICs). This has been met with only partial success: the "defect engineering" of conventional silicon wafers is still an *empirical* exercise. It consists largely of careful, empirical *tailoring* of wafer type (oxygen concentration, crystal growth method, and details of any additional pre-heat treatments, for example) to match the *specific* process details of the application to which they are submitted. Reliable and efficient IG requires the robust formation of near-surface denuded zone (free of oxygen precipitates) and a high precipitate density (at least about 10^8 cm^{-3} [13]) in the wafer bulk. Uncontrolled precipitation of oxygen in the near surface region of the wafer represents a risk to device yield. The denuded zone is conventionally produced by engineering the oxygen concentration profile by oxygen out-diffusion during a pre-anneal at high *T*. But this is not the only way. Considering the sensitivity of oxygen precipitation to vacancy concentration, it is possible to control the denuded zone formation in quite a different way, by profiling the vacancy concentration. This approach now has the name "Magic Denuded Zone^{TM}" or "MDZ^{TM}" [14].

6.2 Vacancy-based oxygen precipitation control schemes

The core of the vacancy-based solution to the oxygen precipitation problem can be seen in the schematic diagram of Fig. 3 first used to illustrate vacancy reactions in crystal growth. The same reactions and vacancy pathways should apply to the processing of wafers as they do to crystal growth.

The part of the diagram labeled "enhanced oxygen precipitation" at temperatures less than about 900 °C, is bounded by a sharp line and drawn at a certain vacancy concentration. This line demarcates the regions of "enhanced oxygen precipitation" from what we might call "normal" behavior. There is indeed a very sharp transition in material behavior. This is the essential feature underlying this method of defect engineering.

Below this bound (denoted by C_V^{cr}) the oxygen precipitation is not enhanced but identical to the nucleation in so-called 'tabula rasa' material. The name derives from the fact that wafers that are pre-annealed around 1000 °C [15] (the tabula rasa treatment) have all crystal growth related ("grown-in") clusters dissolved. From this blank slate, (re-)nucleation at temperatures in the range of about 400–750 °C can proceed in its normal, reproducible, way. The presence of pre-existing grown-in clusters tends to drastically scramble the data from such experiments. The re-nucleation is characterized by a long incubation time, several hours at low temperatures, even if the oxygen concentration is high. Only after sufficient annealing in this temperature range nuclei will grow during subsequent high-temperature anneals. Without it, precipitation is suppressed and oxygen remains in the solution at high temperatures.

The effect of vacancies – introduced in a concentration larger than C_V^{cr} – is mainly to reduce the incubation time down to negligible values. Due to such enormously shortened incubation times in high vacancy concentration material, the nucleation of precipitation nuclei (oxygen clusters) proceeds rapidly even without a special nucleation anneal. When the vacancy-rich wafer is loaded into a furnace for the conventional anneal at 1000 °C, the nucleation occurs efficiently during the temperature ramp-up, if the heating rate is not too fast, as is always the case in conventional furnace treatments. The vacancy effect on incubation is essentially to transfer control of the oxygen precipitation processes from oxygen itself to bound vacancies.

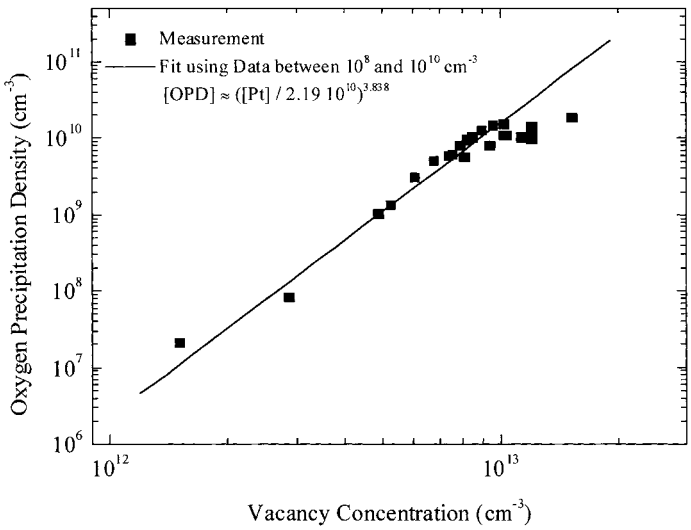

Fig. 9. Oxygen precipitate densities produced following test heat treatments (800 °C/4 h + 1000 °C/16 h) as a function of wafer vacancy concentration. Vacancy concentration was determined by platinum diffusion experiments

Above C_V^{cr} a strong increase in the density of oxygen precipitates produced by standard test heat treatments (such as a two-step anneal: 800 °C/4 h + 1000 °C/16 h) is observed. Figure 9 shows the results of measurements of oxygen precipitate densities resulting from such a test as a function of the measured vacancy concentration in the wafers prior to the precipitation anneal. The measurement of vacancy concentration is discussed below. Within one order of magnitude of vacancy concentration the precipitate density rises above the detection limit of about 10^7 cm^{-3} to over 10^{10} cm^{-3}. The produced precipitate density in the enhanced region is dependent solely and very strongly on the vacancy concentration.

Given the difficulties in controlling the oxygen reaction in the complex heat treatment environments of IC processing outlined above, the use of vacancy concentration potentially offers a very powerful alternative to the usual methods of oxygen precipitation control. The problem is then simply to install an appropriately tailored vacancy concentration in thin silicon wafers and let these vacancies take over the control of the reaction. If properly tailored, the strong, near step-function, relation between vacancy concentration and oxygen precipitate density should produce the layered structure required for the IG system. It turns out that this is surprisingly easy to do.

6.3 The installation of vacancy profiles in silicon wafers

Vacancies may be introduced into silicon wafers at high temperatures by a number of different mechanisms. Two examples are nitridation [16, 17] or simple Frenkel pair generation [14]. Generating large concentrations of vacancies in wafers at high temperatures is not a difficult task at all. The problem lies in keeping the concentration sufficiently large through the cooling down of the wafer such that they may be used subsequently to control nucleation at lower temperatures.

The simplest procedure for installing a useful profile of vacancies in a silicon wafer relies solely on Frenkel pair generation and the close proximity (relative to vacancy diffusion lengths) of the two wafer surfaces. Heating a thin wafer to a high temperature T results in the rapid equilibration of the vacancy–interstitial system. First, Frenkel pairs, vacancies and interstitials in equal amounts, are produced. This very fast reaction leads to recombination–generation equilibrium. The product $C_I C_V$ of the two concentrations acquires the equilibrium value $C_I^* C_V^*$, with the concentration of both equal to $(C_I^* C_V^*)^{1/2}$. If the samples were cooled at this point under the condition of equal concentration, vacancies and interstitials would merely mutually annihilate each other completely in the reverse process of their generation, resulting in no vacancy concentration enhancement by the time the samples reach room temperature.

This is averted by the next stage of the process, that of equilibration. Both C_I and C_V will approach their equilibrium values C_I^* and C_V^*, due to exchange with the wafer surface (considered as ideal sink/source of point defects). This coupled process is controlled mainly by the diffusion of self-interstitials which are the faster diffusers, the two concentrations being comparable. The total time to achieve the complete equilibrium in a standard wafer (about 700 μm thick) was found to be extremely short, less than several seconds at 1250 °C. This implies that the interstitial diffusivity is high, of the order of 2.5×10^{-4} cm^2/s. More discussion of this may be found below, in particular, in the section containing the discussion of Fig. 15.

After equilibration, the vacancies become the dominant species since $C_V^* > C_I^*$, just as it was the case at the melting point. On subsequent cooling the point defects quickly

recombine, only now, vacancies survive. The concentration of the surviving vacancies is identical to the initial concentration difference at the annealing temperature, $\Delta C = C_V^* - C_I^*$. The proximity of the wafer surfaces during cooling adds another component to the process. In addition to recombination, vacancies will out-diffuse to the wafer surfaces where the local (equilibrium) vacancy concentration is rapidly decreasing. However, if the cooling rate is fast enough – in the range of about 40 to 100 K/s (readily accessible through using Rapid Thermal Processing (RTP)) – the middle of the wafer will be not affected by vacancy out-diffusion, and the vacancy species will be present there in the concentration ΔC. The regions near the surfaces will be strongly affected, however. The final freezing-in of the profile is the result of passing through the O_2V binding temperature of about 1020 °C. At this point the vacancies convert from their relatively mobile state (free monovacancies) to their relatively immobile state, O_2V. The profiling of the vacancy concentration through out-diffusion achieved in a given RTP heat treatment is largely the result of the cooling conditions of the wafer above this temperature. Figure 10 illustrates the general features of the process from the perspective of the diagrams used to illustrate crystal growth phenomena. A detailed discussion of the simulation of these effects is presented in a later section.

In the present discussion, the most important thing is that the near-surface regions of a quenched wafer are depleted of vacancies, by vacancy out-diffusion during the cooling stage of RTP. In the near-surface zones the vacancy concentration is below C_V^{cr}, and oxygen precipitation is suppressed in a practical sense as a result of prohibitively long incubation times (the tabula rasa effect). The rapid increase in temperature during the ramp-up to the process temperature serves to dissolve all pre-existing oxygen clusters.

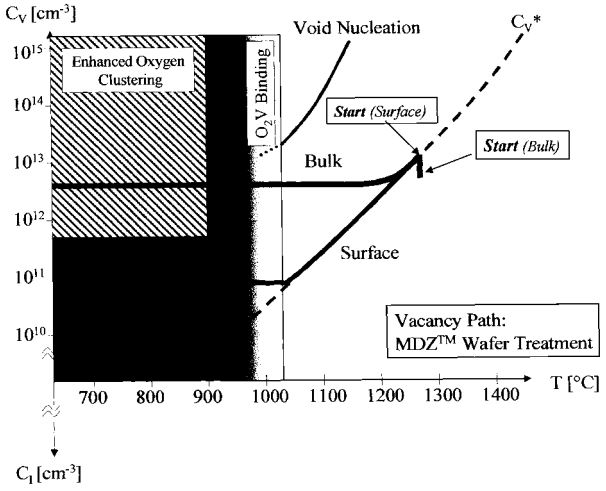

Fig. 10. Schematic diagram using the same vacancy template used to describe vacancy pathways during crystal growth for the problem of the installation of a depth profile of vacancies by high temperature *wafer* heat treatment and rapid cooling. Following rapid Frenkel pair formation whereby $C_V = (C_V^* C_I^*)^{1/2}$ ("start"), the vacancy rises to its equilibrium concentration at the process temperature through interchange with the wafer surfaces, upon cooling it drops due to recombination with the existing interstitials until they are depleted. Following this, and under rapid cooling conditions, only the near surface region effectively interchanges with the surface and the bulk concentration remains unaltered

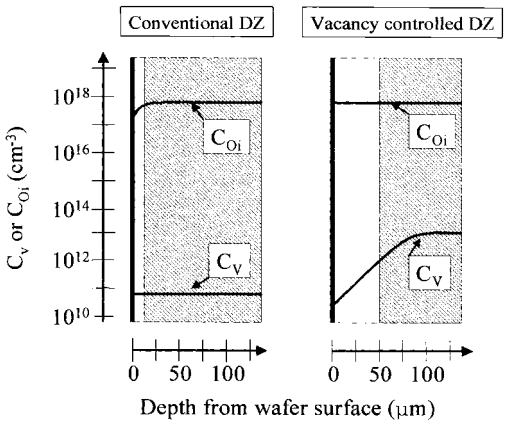

Fig. 11. Schematic illustration of the difference between conventional methods of installing denuded zones (DZ) in silicon wafers via oxygen out-diffusion and renucleation and a new method based on the installation of tailored vacancy concentration profiles

In the middle of a wafer the precipitation is strong, due to the presence of vacancies in a concentration larger than C_V^{cr}. Such a precipitation profile is precisely what is required for ideal IG. The width of DZ (precipitation-denuded zone) is easily controlled by the cooling rate (Fig. 11). Faster cooling rates mean a shorter vacancy diffusion length, and thus a narrower DZ. If the cooling rate is too slow, as occurs in conventional furnace annealing, the high temperature vacancy concentration profile will be allowed to fully relax throughout the sample thickness to its equilibrium value near the binding temperature, which is well below the threshold for precipitation enhancement. At this point the entire wafer thickness becomes of the tabula rasa type and exhibits conventional nucleation behavior.

Installing a vacancy concentration profile which rises from the wafer surface into the bulk of the wafer crossing the critical concentration C_V^{cr} at some desired depth is the core of the MDZ^{TM} concept. The installed vacancies have full control over the oxygen precipitation behavior of the wafer. An example of a depth distribution of oxygen precipitation produced by vacancy concentration control is shown in Fig. 12.

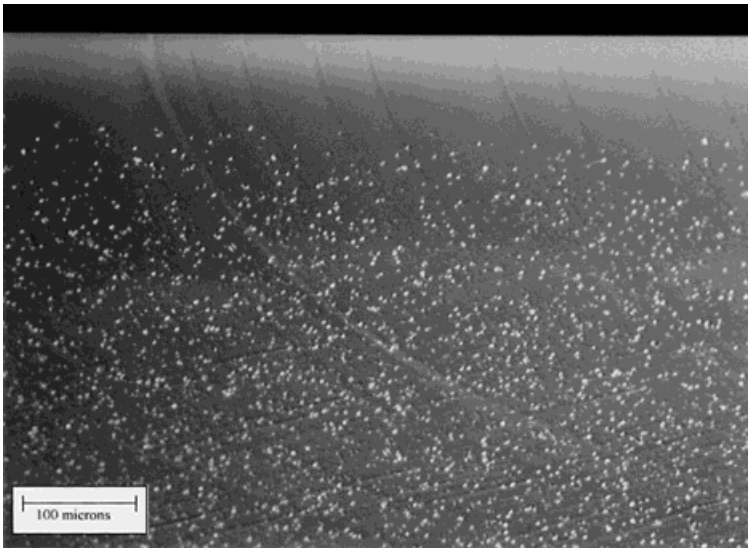

Fig. 12. Etched cross section of a silicon wafer following a precipitation heat treatment (800 °C/4 h + 1000 °C/16 h) showing the depth profile of oxygen precipitates resulting from an RTP-installed vacancy concentration profile. The bulk density of precipitates is 1×10^{10} cm^{-3}

Because of the speed of the vacancy–interstitial recombination reaction and the rapid diffusivities of both vacancies and interstitials (with that of the vacancies being conveniently lower than that of the interstitials), the process which produces an MDZ wafer is very rapid indeed. It is accomplished in several seconds compared to the typically many hours required of the conventional oxygen-based approach. The denuded zones produced are also in general larger than the conventional DZ. Technologically important is the fact that the structure developed is independent of oxygen concentration, crystal growth process, and to a large extent the details of the subsequent thermal processing. The latter result is due to the consumption of vacancies during the very rapid initial nucleation processes. Any subsequent nucleation is then again subject to the "normal" prohibitively long incubation requirements which exist in essentially all practical situations.

6.4 Normal and vacancy-assisted nucleation of oxygen clusters

A possible reason of the 'magic' effect of vacancies (oxygen-independent production of precipitates!) is that oxygen clustering, during the nucleation anneal, proceeds by the agglomeration of vacancy–oxygen species (O_2V). The nucleation rate is controlled by the concentration C_V, and thus independent of the oxygen content. The nucleation rate is a rapidly increasing function of the concentration C_V. Below some critical concentration C_V^{cr}, the nucleation rate becomes negligible.

In the range of low C_V, the agglomerating species are oxygen atoms, and the nucleation rate is then controlled by the oxygen content C. The produced oxygen clusters are strongly strained (unlike the clusters of O_2V species). The free energy gain per atom is $\mu - w$, where $\mu = kT \log (C/C_{OI}^*)$ is the oxygen chemical potential (C_{OI}^* is the oxygen solubility) and w is the strain energy. The difference $\mu - w$ is positive at the nucleation temperature (such as 650 °C) but becomes negative at higher T (at 1000 °C), since μ is then considerably reduced. Thus, the nucleated clusters will all dissolve during the precipitation anneal, regardless of their size. The only way for the clusters to survive is to relieve the strain by emission of self-interstitials. The emission rate becomes fast only if the clusters are larger than some characteristic size. This is considered to be the main reason for a long incubation. During the nucleation stage, the clusters need to grow to a size large enough for subsequent efficient emission of self-interstitials during the precipitation anneal. In the case of clusters of the vacancy–oxygen species O_2V, there is no problem of strain: the space for a cluster is 'carried' by the agglomerating species themselves. Hence there is a negligible incubation time for this vacancy-assisted nucleation.

7. Conclusions Drawn about the Point Defect Parameters from Crystal Growth and Wafer Processing

The problem of the parameters for the intrinsic point defects in silicon is a difficult one. The literature is full of estimates based on a variety of experimental evidence, mostly diffusion data. The scatter in these estimates covers many orders of magnitude.

The analysis of the problem from the point of view of crystal growth and wafer processing experiments described here has the very great advantage of simplicity when compared to many other attempts. In these experiments we are dealing *directly* with

the point defects themselves. The data is not mitigated through a chain of reactions which must be unraveled before the kernel of the problem can be addressed. The high temperatures of the experiments described here insure that we are dealing with for the most part simple unbound point defects. When a deviation from this state occurs, it is immediately apparent. The approach to the problem presented here has the further advantage that it offers a wide variety of experimental observations spanning a relatively large temperature range. There have been other attempts at determining the point defect parameters from crystal growth experiments. In particular we would like to point out the work of Sinno et al. [18], in which a combined approach using both molecular dynamics and experimental data based on the position of OISF-rings was used. The present study takes into account a much wider range of experimental data from both crystal growth (point defect incorporation and agglomeration) and wafer processing.

Each of the effects described above – from crystal growth and wafer processing – add constraints, some strong, some weak, in the range of values of intrinsic point defect parameters which may reasonably describe the observations. These constraints pile up and sharpen the image. It is still a bit of a moving target but while the picture is not yet perfectly sharp the values discussed below give our present best estimates of the point defect parameters. They are the result, essentially, of taking the intersection of the possible ranges of values for the various effects. It is an all-embracing approach to the problem using data from experiments with the point defects in their simplest form. The following sections describe the considerations taken in coming to these conclusions.

7.1 Observations from point defect incorporation and agglomeration phenomena in crystal growth

A typical vacancy growth mode corresponds to the growth rate V about twice as large as the critical value V_{cr}. The incorporated vacancy concentration C_{Vs} is then about half of the highest possible value, $C_{Vm} - C_{Im}$. The incorporated concentration is almost completely spent on the formation of voids, and so it can be deduced from the observed density and volume of voids [6]. The numbers are somewhat scattered giving on average 10^{14} cm^{-3} of vacancies in voids. Accordingly, the difference $C_{Vm} - C_{Im}$ is estimated to be around 2.5×10^{14} cm^{-3}. Next, the vacancy diffusivity D_V (at the nucleation temperature, around 1100 °C) is deduced from the observed void density since the produced void density is very sensitive to the assumed vacancy diffusivity [4]. The result is about 2×10^{-4} cm^2/s at 1100 °C. The room-temperature vacancy diffusivity is deduced from a simple reaction of vacancy diffusion to oxygen traps [19]. Comparing the two numbers, one gets both the vacancy migration energy, 0.35 eV, and the diffusivity extrapolated to the melting point, $D_{Vm} = 4 \times 10^{-5}$ cm^2/s.

Next, the experimental value of the critical V/G ratio (about 2×10^{-5} cm^2/s) imposes constraints on the point defect parameters according to Eq. (1). The critical ratio was also found to be remarkably increased by boron doping which is manifested in shrinking of the OISF-ring [20], that is in expanding the interstitial region at the expense of the vacancy region. This effect is well accounted by a shift in equilibrium concentrations of charged point defects (negatively charged vacancy and positively charged interstitial) [21]. The calculated shift depends strongly on the assumed con-

centration ratio C_{Vm}/C_{Im} (in undoped material), and this was thus fitted to be close to 1.3.

With a known vacancy diffusivity D_{Vm}, the interstitial diffusivity is now obtained from Eq. (1): $D_{Im} = 3.6 \times 10^{-4}$ cm^2/s. In producing this number, the averaged defect formation energy E must be specified. The self-interstitial migration energy is very small [19] and definitely smaller than the migration energy 0.35 eV for vacancies, the slower diffuser. The activation energy for self-diffusion, 4.95 eV [22], is then mostly due to the interstitial formation energy E_I, and we take $E_I = 4.8$ eV as a reasonable value. The vacancy formation energy E_V is under a strong constraint following from the temperature dependence of the $C_V^* - C_I^*$ measured in quenched wafers (discussed in the following section). It is smaller than E_I by about 0.2 eV and so $E_V = 4.6$ eV. An independent estimate of E_V [4] based on the experimental number for the void nucleation temperature (about 1100 °C) is very close to 4.6 eV.

Since D_{Im} is considerably larger than D_{Vm} while the concentrations C_{Im} and C_{Vm} are close to each other, the contribution of the vacancy product $D_{Vm}C_{Vm}$ is of minor importance in Eq. (1).

With specified numbers for ξ_{cr}, E, $C_{Vm} - C_{Im}$ and D_{Vm}, the self-diffusion interstitial product $D_{Im}C_{Im}$ is calculated from (1) to be about 3×10^{11} cm^{-1}s^{-1}. This number is quite close to the value of 2.4×10^{11} cm^{-1} s^{-1} deduced from impurity (Zn, Au) diffusion profiles and from measured self-diffusivity [22]. We prefer the former (a somewhat higher) number which is more consistent with the void-based data.

The numbers listed above are enough to specify the absolute values of the two equilibrium concentrations at the melting point. They give $C_{Vm} = 1.08 \times 10^{15}$ cm^{-3} and $C_{Im} = 8.3 \times 10^{14}$ cm^{-3}.

7.2 Observations from wafer heat treatment phenomena

Installed and measured vacancy concentration profiles in thin silicon wafers can also be used to deduce the point defect parameters and cross check the values deduced from crystal growth. It is a rather straightforward system. The simulation is based on two, coupled, diffusion equations, one for vacancies and one for self-interstitials. The two equations are coupled through rapid vacancy–interstitial recombination. An important feature regarding the transport of vacancies as evident from crystal growth experiments is the binding of vacancies as O_2V [9]. The binding is assumed to be very fast and the number of free vacancies is assumed to be a function only of temperature. The free vacancy concentration is calculated from the total vacancy concentration by

$$C_{V\,\mathrm{free}} = \frac{C_{V\,\mathrm{total}}}{1 + \exp\left(\dfrac{E_b}{k_B}\left(\dfrac{1}{T} - \dfrac{1}{T_b}\right)\right)}, \tag{3}$$

where E_b is the binding energy, T_b the temperature where half of the vacancies are bound to oxygen, k_B is the Boltzmann constant. The bound vacancies are considered immobile on the time scale of RTP.

Another addition to the model takes into account the fact that the silicon wafers used in the present experiment were void-containing. We allowed for diffusion-limited exchange of both self-interstitials (sinking only) and vacancies with these voids. At typical very low densities of voids, the overall effect is negligible but it is included for

completeness. Taking all this into account we obtain the following two equations:

$$\left(\frac{\partial C_{\mathrm{V\,total}}}{\partial t}\right) = \underbrace{\mathrm{div}\,(D_{\mathrm{V}}\,\mathrm{grad}\,C_{\mathrm{V\,free}})}_{\text{V diffusion}} - \underbrace{K_{\mathrm{IV}}\left(C_{\mathrm{V\,free}}C_{\mathrm{I}} - C_{\mathrm{V}}^{*}C_{\mathrm{I}}^{*}\right)}_{\text{I–V recombination}} - \underbrace{4\pi R_{\mathrm{void}}C_{\mathrm{void}}D_{\mathrm{V}}\left(C_{\mathrm{V\,free}} - C_{\mathrm{V}}^{*}\right)}_{\text{release-incorporation of V by voids}}, \tag{4}$$

$$\left(\frac{\partial C_{\mathrm{I}}}{\partial t}\right) = \underbrace{\mathrm{div}\,(D_{\mathrm{I}}\,\mathrm{grad}\,C_{\mathrm{I}})}_{\text{I diffusion}} - \underbrace{K_{\mathrm{IV}}\left(C_{\mathrm{V\,free}}C_{\mathrm{I}} - C_{\mathrm{V}}C_{\mathrm{I}}^{*}\right)}_{\text{I–V recombination}} - \underbrace{4\pi R_{\mathrm{void}}C_{\mathrm{void}}D_{\mathrm{I}}\,\max\left(0, C_{\mathrm{I}} - C_{\mathrm{I}}^{*}\right)}_{\text{recombination of I with voids}}. \tag{5}$$

Note that Eq. (4) describes the time dependence of the total vacancy concentration as a function of the free vacancy concentration.

For the boundary conditions we assume that the concentrations of self-interstitials and free vacancies are equal to their equilibrium concentrations. The initial concentrations were set to $C_{\mathrm{V0}} = 1 \times 10^{10}\,\mathrm{cm}^{-3}$ for vacancies and to $C_{\mathrm{I0}} = 10\,\mathrm{cm}^{-3}$ for self-interstitials over the whole depth. The choice of the initial concentrations has no influence on the concentrations resulting from the simulation of a high temperature step.

7.2.1 Experimental methods

The main tool for probing vacancy concentrations installed in wafers is that of platinum diffusion analysis [23, 24]. The main point is that under appropriate diffusion conditions interstitial platinum $\mathrm{Pt_I}$ is converted to the substitutional state $\mathrm{Pt_s}$, via the Frank-Turnbull mechanism, essentially falling into a vacancy. Substitutional Pt concentration profiles are measured by DLTS. Under these diffusion conditions, the maximum (saturated) $\mathrm{Pt_s}$ concentration is believed to be a good estimate of the vacancy concentration. The situation is complicated somewhat by the fact that at the required Pt diffusion temperatures (about 730 °C) vacancies in the CZ samples investigated here are not free but exist in the form $\mathrm{O_2V}$, and thus conversion of $\mathrm{Pt_I}$ into $\mathrm{Pt_s}$ is accompanied by ejection of an oxygen dimer. There appears to be a small kinetic limitation for the transformation of $\mathrm{Pt_I}$ to $\mathrm{Pt_s}$ via $\mathrm{O_2V}$ compared to free vacancies. At 730 °C several hours diffusion time are required to saturate the $\mathrm{Pt_s}$ concentration. In particular, 5 h seems certainly long enough. At a higher diffusion temperature, such as 800 °C, the saturation in the bulk of the sample (to the same value as found at lower temperatures) is reached much more rapidly. However, near the sample surfaces, where vacancy concentrations are often very low, the Pt diffusion profile deviates strongly from the vacancy concentration profile due to a large "kick-out" diffusion component.

Platinum diffusion and oxygen precipitation data are available for a wide variety of samples treated in different ways. Some of the Pt data, however, were the result of diffusion experiments performed at 730 °C for 20 min, now known to be too short to reach a saturated concentration of $\mathrm{Pt_s}$. Experimentally we have found that the platinum concentration after 5 h at 730 or 800 °C is higher than the concentration after a 20 min diffusion at 730 °C by approximately a factor of 1.9. We have used this factor to adjust older data in the present analysis.

Data from such Pt diffusion experiments were used to produce the graph of Fig. 9 which plots oxygen precipitate density versus Pt concentration. Under the assumption of equality between Pt and vacancy concentration, this graph forms the basis of a second tool for probing vacancy concentration. It is a calibration curve for translating from oxygen precipitation data to vacancy concentration.

7.2.2 Simulations and experimental results

In very rapidly cooled wafers the diffusion of vacancies to the wafer surfaces is not felt by the wafer interior. The frozen-in vacancy concentration here under these cooling conditions is equal to the initial difference of the two equilibrium concentrations, $C_V^* - C_I^*$, the missing vacancies having recombined with the available self-interstitials during cooling. Results from the most recent and carefully made measurements are shown in Fig. 13 for several annealing temperatures.

These points should be compared with the above discussed concentration difference at the melting point $C_{Vm} - C_{im} = 2.5 \times 10^{14}$ cm^{-3}, also included in the plot. If both $C_V^*(T)$ and $C_I^*(T)$ are described by Arrehnius-type dependence, with the activation (formation) energies E_I and E_V, then the plot of Fig. 13 puts constraints on the possible values of the formation energies. Generally speaking, one can specify any number in the range from 3.2 to 4.8 eV for E_I and get a good fit of the experimental points in Fig. 13, but only within a very narrow range of E_V, around the best-fit value $E_V(E_I)$. This best-fit value is very close to E_I; the difference $E_V - E_I$ is small and negative at higher E_I, and small and positive at lower E_I. Therefore, it is certain that the two formation energies are almost identical. As pointed out above, we accept $E_I = 4.8$ eV and then get $E_V = 4.6$ eV to fit the points in Fig. 13. The corresponding temperature dependence of $C_V^* - C_I^*$ is shown by a solid line in Fig. 13.

Wafer heat treatment experiments are especially suited for gathering evidence regarding the diffusivities of the two point defect species. Several experiments representative of a wide range of experiments performed to probe the point defect parameters are described below. Using the precise temperature–time profile of the particular RTA systems used, a good overall fit to this wide range of experiments is achieved using the parameter set shown in Table 1. The numbers in this table are in turn consistent with all other experimental data discussed above. We continue to make small adjustments to these values as new experimental evidence arises but they are not moving very far any

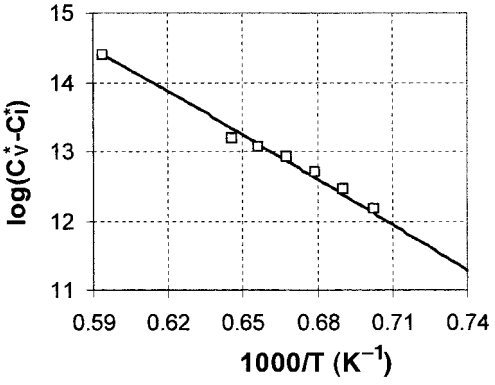

Fig. 13. Measured difference of the equilibrium concentrations of vacancies and self-interstitials ($C_V^* - C_I^*$) at several temperatures, incorporating the data from crystal growth and wafer heat-treatment experiments

Table 1
Point defect parameters used for the vacancy profile calculations

parameter	melting point value	activation energy (eV)
C_V^*	1×10^{15} cm^{-3}	4.5
C_I^*	7.7×10^{14} cm^{-3}	4.7
D_V	7×10^{-5} cm^{-2} s^{-1}	0.35
D_I	3×10^{-4} cm^{-2} s^{-1}	0.25
K_{IV}	10^{-11} cm^3 s^{-1}	1.0

Void parameters: $C_{void} = 3 \times 10^6$ cm^{-3}; $R_{void} = 55$ nm;
oxygen binding: $T_b = 1070$ °C; $E_b = 5$ eV

more. The results are not sensitive to the value of the recombination rate constant K_{IV}, provided it is fast enough, and a tentative number in the table satisfies this condition. We cannot judge the actual value of K_{IV} from these experiments except to set lower limits.

Figure 14 shows a typical plot of simulated vacancy profiles, together with the experimental results. The wafer was treated at 1250 °C for 30 s and cooled rapidly at an average cooling rate of about 50 K/s. The data represent the results of a 5 h 730 °C Pt diffusion (as well as of diffusion at 800 °C performed on a similar sample heated for 20 s). Also shown is the depth profile of oxygen precipitation resulting from a two-step anneal of 4 h at 800 °C + 16 h at 1000 °C. The precipitate density scale has been chosen such that the precipitate density can also be read as the vacancy concentration through the data of Fig. 9. The calculated profile of the resulting frozen-in vacancy concentration is quite good using the parameters of Table 1.

The problem can be broken down into smaller parts which can be investigated individually, to give a better idea of the quality of the individual fits of vacancy and interstitial diffusivity and the vacancy binding parameters. For example, as discussed above, in the initial phase of these treatments as a silicon wafer is heated, vacancies and self-

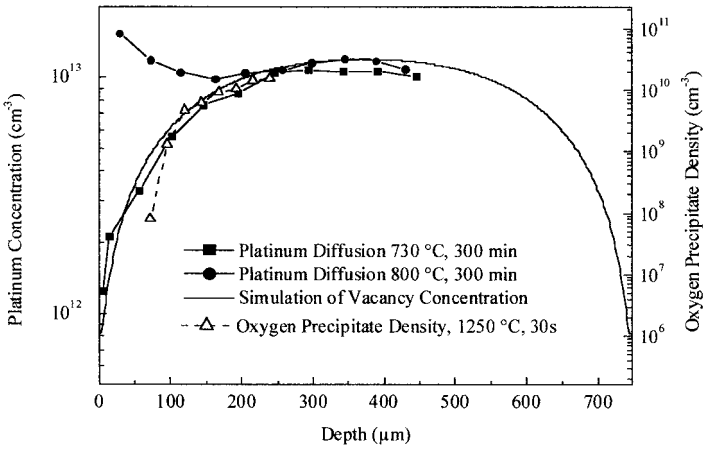

Fig. 14. Depth profiles of platinum diffusion profiles measured at 730 and 800 °C, calculated vacancy concentrations and measured oxygen precipitate densities in an RTP-treated sample processed at 1250 °C. The oxygen precipitate density axis is scaled to correspond to the vacancy-precipitate density calibration

interstitials are created in equal concentrations as Frenkel pairs. Through diffusive transport to the surface these initially equal concentrations become equilibrated in time to their respective equilibrium concentrations, C_V^* and C_I^* at the annealing temperature. The transport in this coupled diffusion process will be dominated by the self-interstitial diffusivity. The time required to achieve equilibration is largely a measure of this number. Experimental evidence shows this equilibration time to be very fast at typical process temperatures of >1200 °C. Equilibration is found to be very nearly complete in the fastest possible times RTP systems can heat and cool wafers. There appears, however, to be a small signal of slight deviation from equilibration in very short times at the process temperature. Figure 15 shows the result of Pt diffusion and corresponding oxygen precipitate data taken on samples processed for variable hold times at a process temperature of 1250 °C. The fact that the simulated vacancy concentration fits this well is an indication that the interstitial diffusivity used cannot be too far off the mark.

The development of the profile *shape* of vacancy concentration which arises during the cooling phase of the treatment is, on the other hand, largely controlled by vacancy diffusivity. The minority interstitial concentration rapidly disappears as soon as the temperature begins to drop. Figure 14 already demonstrated that the parameters used for vacancy diffusion and binding result in very good agreement. More evidence in support of this is given in Figs. 16 and 17. These figures illustrate the results of experiment and calculation of the effects of changing the cooling rate following 1250 °C treatments. Figure 16 shows the values of the resulting oxygen precipitate densities (a measure of the vacancy concentration as described above) in the center of the wafer as a function of cooling rate. This then is a measure of the extent to which the vacancy out-diffusion profile has penetrated to the middle of the sample as the cooling rate slows down. Again, calculation with this parameter set shows rather good agreement with the data. Figure 17 contains information about the *shape* of the out-diffusion profile in the same samples as Fig. 16. Plotted are the positions of the measured denuded zone as a function of cooling rate. "Denuded zone" is of course a somewhat slippery concept. The edge of the denuded zone is not easy to define. What is meant is the position in space

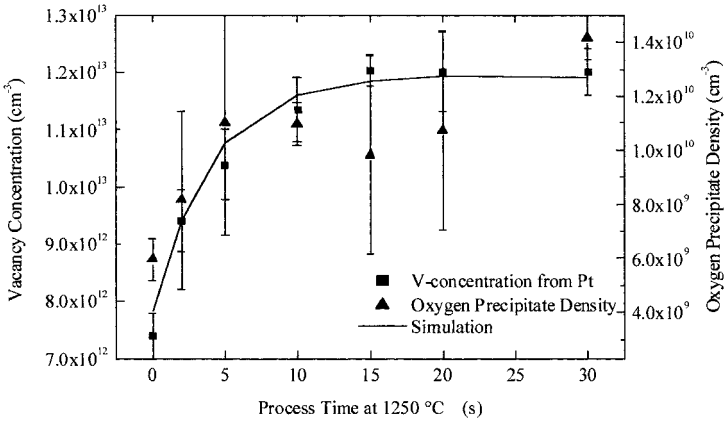

Fig. 15. Vacancy concentrations determined by Pt diffusion, calculated vacancy concentration and oxygen precipitate densities in the wafer center following heat treatments at 1250 °C for a range of soak times

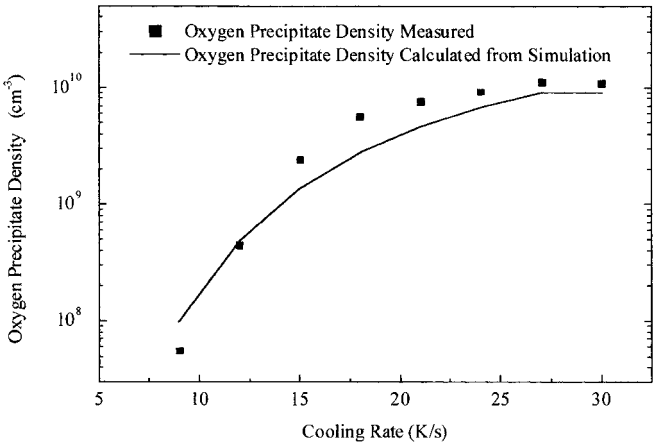

Fig. 16. Results of a study of the effects of cooling rate following vacancy installation treatments at 1250 °C at a variety of cooling rates. Plotted are the measured oxygen precipitate densities at the wafer centers and the calculated oxygen precipitate densities from vacancy concentration calculations scaled to oxygen precipitate densities

of where the density of oxygen precipitates drops below the detection limit. But what is the detection limit? This depends on the volume (surface area and etch depth) observed, and is not a standard concept. It is thus difficult to accurately compare reports of denuded zone measurements. The determination of this detection limit is not easy especially when faced with spatially varying precipitate counting. With this in mind, we have in Fig. 17 plotted our measurements of denuded zone position – performed in an internally consistent manner – with calculations of the positions of *two* different vacancy concentrations (2 and 3.5×10^{12} cm^{-3}) for each of the cooling rates. The best fit, and it is a rather good one, is for the edge of the denuded zone corresponding to a

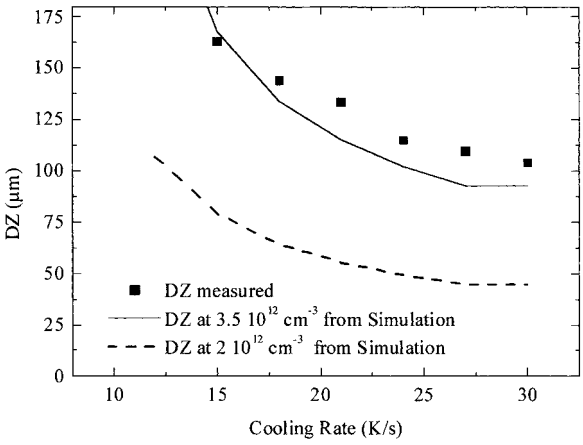

Fig. 17. Results of a study of the effects of cooling rate following vacancy installation treatments at 1250 °C at a variety of cooling rates. Plotted are the resulting measured denuded zone depths (DZ) in the samples and calculated denuded zone depths for DZ corresponding to 2×10^{12} and 3.5×10^{12} cm^{-3}

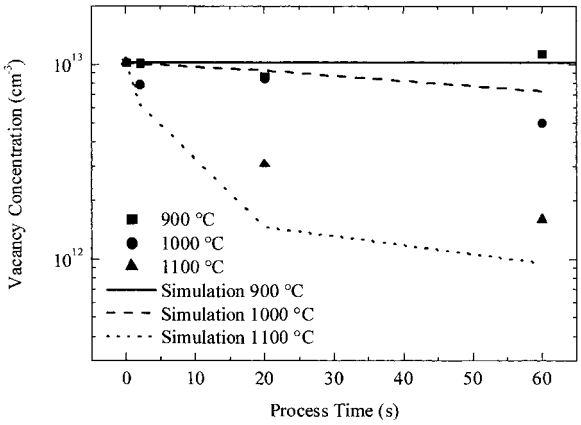

Fig. 18. Results of a study of the relaxation of 1250 °C installed vacancy concentration profiles at three lower temperatures 900, 1000 and 1100 °C for a variety of times. In these experiments, two-step heat treatments were used to first set a "standard" profile (at 1250 °C) and then to relax this profile at a variety of second temperatures for various times. Only the value of vacancy concentration at the center of the wafer following the two-step treatment is given here

vacancy concentration of 3.5×10^{12} cm^{-3}. This would make the measured value for the denuded zone correspond to about 2×10^{8} cm^{-3} in these examples.

Finally, the importance of the binding of vacancies can be illustrated and the parameters probed using a different kind of experiment. In these experiments we perform a two-step heat treatment. In the first step, we *install* vacancy profiles into wafers using standard 1250 °C rapidly cooled treatments. We then re-heat the wafers to one of three new temperatures, 1100, 1000 or 900 °C for varying lengths of time and then cool rapidly again. The idea is to observe the time evolution of the profile *relaxation* to its new value for the lower temperature state. Again, calculations were performed using the complete temperature profile in time for the treatments. Figure 18 shows vacancy concentration measurements taken from the center of the wafers and calculations of the same following a two-step heat treatment. At 900 °C the vacancy profile is nearly immobile. Results of detailed concentration profile measurements confirm this. Further experiments in which the second heat treatment was performed at 900 °C for times as long as 15 min confirm that within the accuracy of our measurements the profile has not moved.

Again, the parameters in Table 1 do a reasonably good job of fitting the data. These particular examples were chosen to illustrate just how important the binding of vacancies is in explaining the wafer results, just as they were in explaining crystal growth results. The following example will serve to illustrate the point in another way. Under the assumption of no binding effect, fitting the relaxation data as well as is possible results in completely unrealistic vacancy diffusion behavior. Migration energies on the order of 3 eV and a melting point value of about 10^{-3} cm^2/s result.

It is expected that experiments of this type will lead to a more precise determination of the binding parameters. At the moment we can say that the binding temperature lies within the range of about 1020 to 1070 °C.

8. Conclusions

The main conclusions regarding the properties of intrinsic point defects in silicon derived from the work described above can be summarized as follows:

1. Recombination of vacancies and self-interstitials at high temperatures is a very fast process. It is surely faster than 1 s at 1200 °C corresponding to a recombination constant K_{IV} of about 10^{-12} cm^3/s.

2. The properties of the two intrinsic point defects vacancies and self-interstitials are very similar. The main difference is in the diffusivity of the two species. It is larger for self-interstitials, but only by a factor of about ten.

3. The migration energies of both point defects are very low, about 0.35 eV for vacancies and still less for self-interstitials, although the precise number is not well established.

4. On the other hand, the formation energies of both are very large (4.8 eV for self-interstitials and 4.6 eV for vacancies). This feature is very important. It is required to explain the nucleation of microdefects in crystal growth. Small formation energies are inconsistent with the levels of supersaturation required to drive the nucleation of voids or dislocation loops at the temperature where they are observed to occur.

5. The equilibrium concentrations of the two point defects at the melting point are very similar. The difference is only about 30%. For this reason the critical V/G ratio for the change over from interstitial to vacancy dominance is very sensitive to charged impurities, especially dopants. Already at moderate concentrations, less than about 10^{19} cm^{-3}, boron produces large upward shifts in this critical value. A similar, but oppositely directed effect is expected for donor dopants.

6. A crucial component of the point defect system is the binding of vacancies by oxygen to form O_2V. Without this vacancy storage mechanism, in all realistic cases, vacancy consumption to voids or surfaces would go to completion, or nearly so. Residual vacancies (necessary to explain enhanced oxygen precipitation phenomena in both crystals and wafers) could not be explained.

7. Vacancies stored in the form of O_2V in concentration larger than about 1×10^{12} cm^{-3} strongly enhance oxygen precipitation mainly through a drastic reduction of incubation times. This is explained by a mechanism in which a different path to nucleation emerges in which O_2V species and not oxygen atoms are involved as the agglomerating species. In this way the reaction becomes de-coupled from the oxygen concentration.

Acknowledgements Computer programs for the simulation of point defect dynamics during MDZ^{TM} treatments were developed in part by Marco Pagani. We also wish to acknowledge the contributions of Jeff Libbert, Daniela Gambaro, Max Olmo, Paolo Mutti and Lucio MuléStagno of MEMC Electronic Materials, Peter Pichler of the Fraunhofer Instititut, Erlangen and Harold Korb to this work.

References

[1] V.V. Voronkov, J. Cryst. Growth **59**, 625 (1982).
[2] V.V. Voronkov and R. Falster, J. Appl. Phys. **86**, 5975 (1999).
[3] M. Hasebe, Y. Takeoka, S. Shinoyama, and Saito, Jpn. J. Appl. Phys. **28**, L1999 (1989).
[4] V.V. Voronkov and R. Falster, J. Cryst. Growth **194**, 76 (1998).
[5] N.I. Puzanov and A.M. Eidenzon, Semicond. Sci. Technol. **7**, 406 (1992).
[6] T. Saishoji, K. Nakamura, H. Nakajima, T. Yokoyama, T. Ishikawa, and J. Tomioka, ECS Proc. **98–13**, 28 (1998).
[7] T. Ueki, M. Itsumi, and T. Takeda, Appl. Phys. Lett. **70**, 1248 (1997).
[8] J.G. Park, G.S. Lee, J.M. Park, S.M. Chon, and H.K. Chung, ECS Proc. **99-1**, 324 (1999).
[9] V.V. Voronkov and R. Falster, J. Cryst. Growth **204**, 462 (1999).
[10] R. Falster, V.V. Voronkov, J.C. Holzer, S. Markgraf, S. McQuaid, and L. MuléStagno, ECS Proc. **98-1**, 468 (1998).
[11] A.J.R. de Kock, Philips Res. Rep. Suppl. **1**, 1 (1973).
[12] R. Falster and V.V. Voronkov, Mater. Sci. Eng. B **73**, 87 (2000).

[13] R. FALSTER, G.R. FISHER, and G. FERRERO, Appl. Phys. Lett. **59**, 809 (1991).
[14] R. FALSTER, D. GAMBARO, M. OLMO, M. CORNARA, and H. KORB, Mater. Res. Soc. Symp. Proc. **510**, 27 (1998).
[15] R. FALSTER, M. CORNARA, D. GAMBARO, M. OLMO, and M. PAGANI, Solid State Phenom. **57/58**, 123 (1997).
[16] R. FALSTER, M. PAGANI, D. GAMBARO, M. CORNARA, M. OLMO, G. FERRERO, P. PICHLER, and M. JACOB, Solid State Phenom. **57/58**, 129 (1997).
[17] M. JACOB, P. PICHLER, H. RYSSEL, R. FALSTER, M. CORNARA, D. GAMBARO, M. OLMO, and M. PAGANI, Solid State Phenom. **57/58**, 349 (1997).
[18] T. SINNO, R.A. BROWN, E. DORNBERGER, and W. VON AMMON, J. Electrochem. Soc. **145**, 303 (1998).
[19] G.D. WATKINS, ECS Proc. **99-1**, 38 (1999).
[20] E. DORNBERGER, D. GRAF, M. SUHREN, U. LAMBERT, P. WAGNER, F. DUPRET, and W. VON AMMON, J. Cryst. Growth **180**, 343 (1997).
[21] V.V. VORONKOV and R. FALSTER, J. Appl. Phys. **87**, 4126 (2000).
[22] H. BRACHT, ECS Proc. **99-1**, 357 (1999).
[23] H. ZIMMERMANN and H. RYSSEL, Appl. Phys. Lett. **59**, 1209 (1991).
[24] M. JACOB, P. PICHLER, H. RYSSEL, and R. FALSTER, J. Appl. Phys. **82**, 182 (1997).